CHEMISTRY OF MATERIALS
Cite This: Chem. Mater. 2018, 30, 421−427
Article
pubs.acs.org/cm

Potential Semiconducting and Superconducting Metastable Si_3C Structures under Pressure

Guoying Gao,*[,†,§] Xiaowei Liang,[†] N. W. Ashcroft,[‡] and Roald Hoffmann*[,§]

[†]State Key Laboratory of Metastable Materials Science and Technology, Yanshan University, Qinhuangdao 066004, China
[‡]Laboratory of Atomic and Solid State Physics, Cornell University, Ithaca, New York 14853, United States
[§]Department of Chemistry and Chemical Biology, Cornell University, Ithaca, New York 14853, United States

Supporting Information

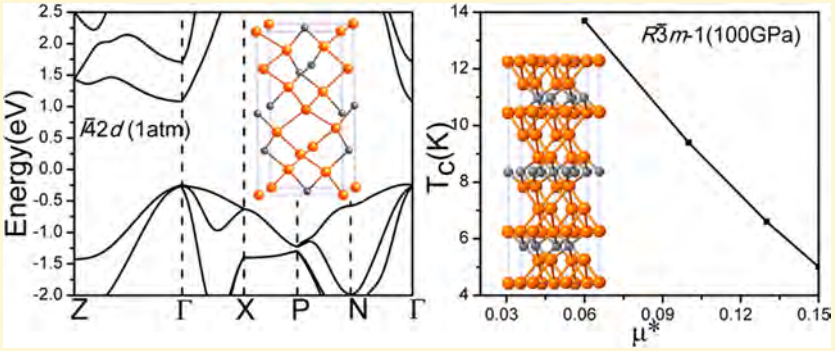

ABSTRACT: Si_3C is predicted to take on a diamond type structure (space group: $I\bar{4}2d$), at P = 1 atm, consistent with the experimental results on a cubic $Si_{0.75}C_{0.25}$ alloy. This structure is computed to be a semiconductor with a direct band gap of about 1.3 eV, within the desired values. Under pressure, Si_3C may transform to metastable metallic $R\bar{3}m$-2 and $R\bar{3}m$-3 structures at about 25 and 250 GPa, respectively. Both are layered structures with six-coordinate Si and unusual six-coordinate carbon atoms. The $R\bar{3}m$-1 and $R\bar{3}m$-2 structures are both estimated to be superconductors with T_c of a few Kelvin. This is the first time that superconductivity in undoped silicon carbides is calculated.

INTRODUCTION

As the second most abundant element in the Earth's crust, relatively low cost, and an intrinsic semiconductor that can be both *n* and *p* doped, silicon has been widely used in the electronic industry. The well-known diamond type Si(d-Si) structure is a semiconductor with an indirect gap of 1.2 eV and a much larger direct gap of 3.4 eV.[1] As a consequence of the indirect gap nature of d-Si, Si solar cell absorber layers need to be relatively thick to absorb low energy photons. Much theoretical and experimental work[2,3] has been directed toward the design and synthesis of direct band gap silicon allotropes, at 1 atm and under high pressure, preferably with a band gap value around optimal (1.1−1.4 eV) for effective solar light conversion.[4] Some of the silicon allotropes designed or made so far do approach a direct band gap.[5]

For carbon, graphite and diamond are, respectively, a semimetal and an insulator with a large indirect band gap of 5.48 eV. If we mix silicon and carbon, there is a possibility that we might get some compounds with the desirable direct band gap within 1.1−1.4 eV. As the only thermodynamically stable composition in the silicon/carbon system, SiC (in its many polytypes) is indeed a semiconductor, but with the still large and indirect band gap of 2.4 eV.

In the Si/C phase diagram, only SiC is stable at P = 1 atm.[6] There are some reasons to explore Si:C compositions other than 1:1, even if they may only be metastable. One is close to organic chemistry here, where the size of barriers to rearrangement and decomposition is large, and so substances that are metastable may be nevertheless persistent. In addition to SiC, several alloys or solid solutions, such as $Si_{0.75}C_{0.25}$,[7] $Si_{80}C_{20}$,[8,9] and $Si_{5.04}C_{2.96}$,[10,11] have been synthesized. The similar $Si_{0.75}Ge_{0.25}$,[12,13] $Si_{80}Ge_{20}$,[14,15] $Si_{0.5}Ge_{0.5}$[16] alloys or solid solutions are also known. Among them, a $Si_{0.75}C_{0.25}$ alloy was observed in the products resulting from thermal reduction of molybdenum disilicide heating rods and was proposed to have a cubic structure with Si and C atoms residing on sites of the diamond crystal structure.[7] There is still no detailed study of this Si_3C form. In a previous contribution we investigated this composition at P = 1 atm and found several metastable structures.[17] In this paper we return to the Si_3C composition, in the context of a search for a semiconductor with direct band gap of around 1.4 eV and, at elevated pressure, the potential for superconductivity.

Received: October 9, 2017
Revised: December 14, 2017
Published: December 14, 2017

DOI: 10.1021/acs.chemmater.7b04243
Chem. Mater. 2018, 30, 421−427

COMPUTATIONAL METHODS

We employ the well-developed CALYPSO structure prediction method, which is designed to search for the stable structures of given compounds.[18−22] The underlying energetic calculations are performed with the plane-wave pseudopotential method as implemented in the VASP code.[23] The Perdew−Burke−Ernzerhof generalized gradient approximation[24] is chosen for the exchange-correlation functional. The electron−ion interaction is described by projector-augmented-wave potentials with the $3s^2 3p^2$ and $2s^2 2p^2$ configurations treated as valence electrons for Si and C, respectively. A kinetic cutoff energy of 600 eV and corresponding Monkhorst−Pack (MP) k-point meshes for different structures are then adopted to ensure that the enthalpy converges to better than 1 meV/atom. The Crystal Orbital Hamiltonian Population (COHP)[25,26] formalism was used for bond analysis, as implemented in the LOBSTER package.[27]

The phonons were computed by using a supercell approach[28] within the PHONOPY code.[29] We used 2 × 2 × 2, 2 × 2 × 2, 2 × 2 × 2, 2 × 2 × 2, and 4 × 4 × 1 supercells for $I\bar{4}2d$, $R\bar{3}m$-1, $R\bar{3}m$-2, $R\bar{3}m$-3, and $P3m1$-1, respectively. The electron−phonon coupling (EPC) of the stable compounds is calculated within the framework of linear response theory through the Quantum-ESPRESSO code.[30] Norm-conserving pseudopotentials for Si and C were employed, and convergence tests concluded that suitable values would be a 60 Ry kinetic energy cutoff. A 6 × 6 × 6 q-point mesh in the first Brillouin zone (BZ) for $R\bar{3}m$-1 and $R\bar{3}m$-2 Si_3C was used in the EPC calculation. A MP grid of 36 × 36 × 36 and 24 × 24 × 24 was used to ensure k-point sampling convergence with Gaussians of width 0.03 Ry for $R\bar{3}m$-1 and $R\bar{3}m$-2, respectively, which approximates the zero-width limits in calculations of the EPC parameter λ.

RESULTS AND DISCUSSION

We carried out a detailed structure search on the Si_3C composition by CALYPSO[18−22] at 1 atm and 50, 100, 200, and 300 GPa, with simulation cells containing up to eight Si_3C formula units. At 1 atm, our previous theoretical work[17] on Si_3C predicted a diamond type structure with doubled cell (Figure 1a). This is consistent with experimental observations

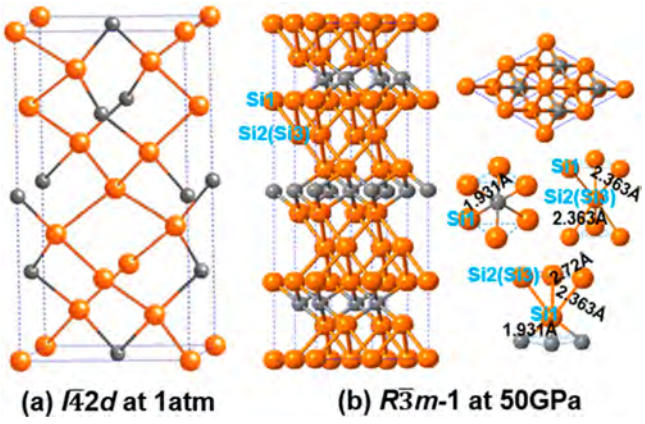

Figure 1. Predicted $I\bar{4}2d$ and $R\bar{3}m$-1 structures for Si_3C at 1 atm and 50 GPa, respectively. Orange, large balls are Si; gray, small balls carbon. The right panel of (b) presents the top view of the $R\bar{3}m$-1 structure and Si- or C-centered octahedra within the structure.

on the $Si_{0.75}C_{0.25}$ alloy, which also points to a cubic structure with Si and C atoms residing on sites of the diamond crystal structure. The calculated lattice parameter of the predicted $I\bar{4}2d$ Si_3C structure along [100] and [010] is 4.8 Å, which is close to 4.9 Å reported in the $Si_{0.75}C_{0.25}$ alloy.[7] The main difference is the periodicity along the diamond [001] direction. The $Si_{0.75}C_{0.25}$ alloy cell was reported to be 2.5 times the diamond unit cell in the previous study, while it is 2 times in our predicted $I\bar{4}2d$ Si_3C structure. We have been unable to build up a cubic structure with 2.5 times of the diamond unit cell. It is also possible that 10 periods of the diamond unit cell or not orthogonal unit cell exist. In addition, the experimentally observed $Si_{0.75}C_{0.25}$ alloy might be fully disordered with Si/C mixed sites. These uncertainty needs to be reexamined by further experiment.

In our calculations for Si_3C we also obtained a diamond type structure, but also, over the whole pressure range studied (1 atm to 300 GPa), we predict another phase, a metastable $R\bar{3}m$-1 one for Si_3C. We show this very different structure in Figure 1b. The layering of the $R\bar{3}m$-1 structure is evident; we describe the bonding in this phase in the Supporting Information. The structure shows SiC and Si layers, hinting at still further segregation.

Our search indeed leads to two optimum $R\bar{3}m$-2 and $R\bar{3}m$-3 structures (Figure 2a,b) with more extensive segregation under

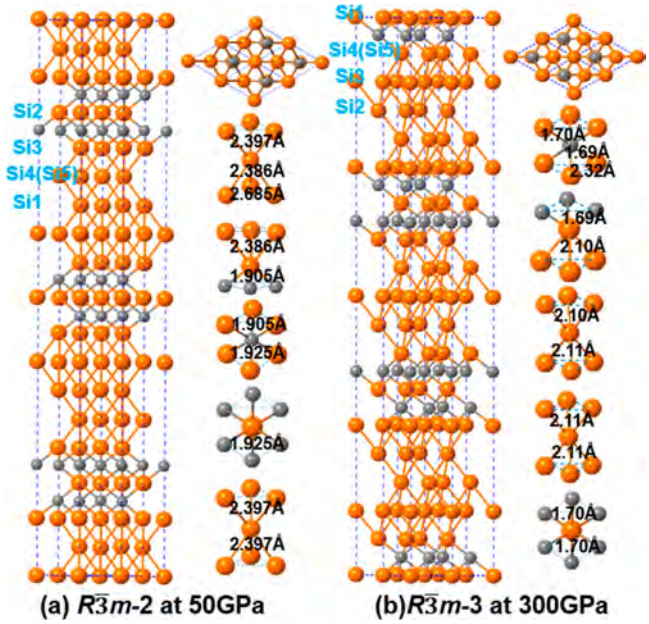

Figure 2. Predicted $R\bar{3}m$-2 and $R\bar{3}m$-3 structures for Si_3C at 50 and 100 GPa, respectively. Orange, large balls are Si; gray, small balls carbon.

pressure. We also found a number of other metastable structures under pressure, such as $P\bar{3}m1$, $P3m1$-1, $P3m1$-2, $R3m$, and $P6_3/mmc$ (see Figure S1 in the SI). Detailed information on the crystal structures found is given in Table 1; all are layered structures, partially segregated. As a reviewer suggested, any bulk synthesis will likely create a random stacking of SiC and Si layers, deviating from the Si_3C composition. Therefore, one needs to control the ratio between SiC and Si during the experimental synthesis process.

The octahedral coordination geometries of Si and C in the predicted structures for Si_3C are intriguing. They do not occur for elemental C until terapascal pressures.[31−33] Elemental Si undergoes a series of phase transitions, with six-coordination initiated in the β-Sn structure at about 10 GPa. SiC transforms in calculations to a six-coordinate (at both Si and C) rock salt structure at around 68 GPa, consistent with the inherent ionicity and the necessity of moving to higher coordination. Experimentally, this transition does not take place until ∼100 GPa at room temperature[34,35] or 40 GPa at high temperature.[36] The Si−C distances in Si_3C are 1.69−1.931 Å, a little longer than SiC at corresponding pressures (1.79 Å at 50 GPa for the diamond type phase, 1.59 Å at 300 GPa for sodium chloride phase). The Si atoms in the $R\bar{3}m$-1 and $R\bar{3}m$-3 structures are octahedrally

DOI: 10.1021/acs.chemmater.7b04243
Chem. Mater. 2018, 30, 421−427

Table 1. Space Group, Lattice Parameters (Å), and Atomic Wyckoff Positions of Si_3C

pressure	space group	lattice parameter (Å)	atomic positions
1 atm	$I\bar{4}2d$ (No. 122)	$a = b = 4.953$	Si1(8d) (0.68393, 0.25, 0.125)
		$c = 9.6$	Si2(4a) (0, 0.5, 0.25)
			C(4b) (0, 0.5, 0.75)
50 GPa	$R\bar{3}m$-1 (No. 166)	$a = b = 2.718$	Si1(6c) (0, 0, 0.23152)
		$c = 17.346$	Si2,Si3(3a) (0, 0, 0)
		$\gamma = 120°$	C(3b) (0, 0, 0.5)
50 GPa	$R\bar{3}m$-2 (No. 166)	$a = b = 2.685$	Si1(3a) (0, 0, 0)
		$c = 35.32$	Si2(3b) (0, 0, 1/2)
		$\gamma = 120°$	Si3(6c) (0, 0, 0.89694)
			Si4,Si5(6c) (0, 0, 0.61493)
			C(6c) (0, 0, 0.80104)
50 GPa	$P3m1$-1 (No. 156)	$a = b = 2.68$	Si1(1c) (2/3, 1/3, 0.49742)
		$c = 11.81$	Si2(1c) (2/3, 1/3, 0.80760)
		$\gamma = 120°$	Si3(1b) (1/3, 2/3, 0.18859)
			Si4(1a) (0, 0, 0.65392)
			Si5(1a) (0, 0, 0.34150)
			Si6(1a) (0, 0, 0.99794)
			C1(1c) (2/3, 1/3, 0.09471)
			C2(1b) (1/3, 2/3, 0.90109)
50 GPa	$R3m$ (No. 160)	$a = b = 2.689$	Si1(3a) (0, 0, 0.94891)
		$c = 35.306$	Si2(3a) (0, 0, 0.44961)
		$\gamma = 120°$	Si3(3a) (0, 0, 0.38460)
			Si4(3a) (0, 0, 0.56391)
			Si5(3a) (0, 0, 0.66716)
			Si6(3a) (0, 0, 0.1799)
			C1(3a) (0, 0, 0.81501)
			C2(3a) (0, 0, 0.08320)
50 GPa	$P\bar{3}m1$ (No. 164)	$a = b = 2.691$	Si1(2d) (2/3, 1/3, 0.76804)
		$c = 11.777$	Si2(2d) (2/3, 1/3, 0.42373)
		$\gamma = 120°$	Si3(2d) (1/3, 2/3, 0.92161)
			C(2c) (0, 0, 0.66990)
50 GPa	$P6_3/mmc$ (No. 194)	$a = b = 2.728$	Si1(2c) (2/3, 1/3, 3/4)
		$c = 11.479$	Si2(4f) (2/3, 1/3, 0.09751)
		$\gamma = 120°$	C(2a) (0, 0, 1/2)
50 GPa	$P3m1$-2 (No. 156)	$a = b = 2.691$	Si1(1b) (1/3, 2/3, 0.97962)
		$c = 11.780$	Si2(1b) (1/3, 2/3, 0.63587)
		$\gamma = 120°$	Si3(1a) (0, 0, 0.13512)
			Si4(1a) (0, 0, 0.82680)
			Si5(1a) (0, 0, 0.48139)
			Si6(1c) (2/3, 1/3, 0.28848)
			C1(1b) (1/3, 2/3, 0.38330)
			C2(1c) (2/3, 1/3, 0.73015)
300 GPa	$R\bar{3}m$-3 (No. 166)	$a = b = 2.324$	Si1(3a) (0, 0, 0)
		$c = 32.067$	Si2(3b) (0, 0, 1/2)
		$\gamma = 120°$	Si3(6c) (0, 0, 0.88426)
			Si4,Si5(6c) (0, 0, 0.26829)
			C(6c) (0, 0, 0.36599)

coordinated by Si and C, or just Si or C alone, while some of the Si atoms in the $R\bar{3}m$-2 phase are five-coordinated by just Si.

Why are the Si−C distances in Si_3C longer than in SiC? Under compression, the only structural imperative for atoms is to get on average closer together. This is the rationale for the general increase in coordination. The number of electrons per atom does not change. So more atoms are bonded by the same number of electrons, a situation known as electron-deficient multicenter bonding. This is exactly what happens for boron in its elemental structure and in its compounds, at ambient pressure.[37]

Enthalpy calculations as a function of pressure show that the diamond type $I\bar{4}2d$ structure for Si_3C is the most stable at 1 atm and remains such up to 25 GPa, above which the $R\bar{3}m$-2 phase becomes stable. At 250 GPa, another $R\bar{3}m$-3 structure is preferred. Among all the predicted structures, only the diamond type $I\bar{4}2d$ structure is stable relative to solid elements, and that in a very small pressure range, around 10 GPa.

The reaction enthalpies calculated are summarized in Figure 3. As anticipated, all the predicted structures are unstable with respect to solid silicon and SiC over the whole pressure range studied. However, the diamond type $I\bar{4}2d$ and $R\bar{3}m$-1 phases might be synthesized as metastable structures, since they are dynamically stable at 1 atm; the diamond type structure remains such up to 50 GPa, and $R\bar{3}m$-1 up to at least 300 GPa (Figure S3). The $R\bar{3}m$-2 and $R\bar{3}m$-3 phases are dynamically stable between

DOI: 10.1021/acs.chemmater.7b04243
Chem. Mater. 2018, 30, 421−427

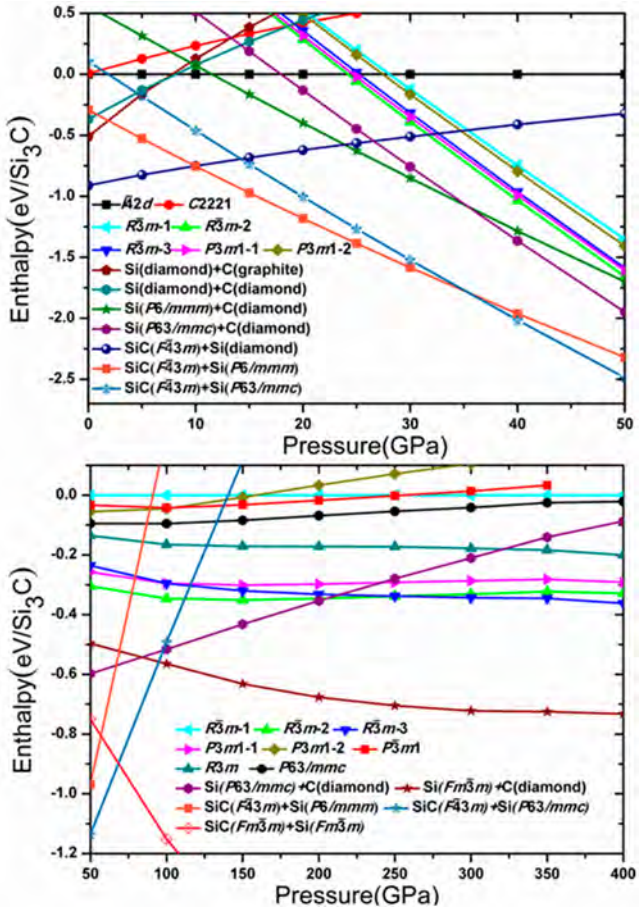

Figure 3. Ground-state static enthalpy curve per formula unit as a function of pressure for Si_3C, with respect to the diamond-type $I\bar{4}2d$ (upper panel) and $R\bar{3}m$-1 (lower panel) structure, respectively. The decomposition enthalpies for Si_3C to Si+C and SiC+Si are also presented. We considered diamond-type $F\bar{4}3m$, $P6/mmm$, $P6_3/mmc$, and $Fm\bar{3}m$ structures for Si, graphite, and diamond for C and $F\bar{4}3m$ and $Fm\bar{3}m$ for SiC, respectively.

25 and 250 GPa and 100−400 GPa, respectively. Moreover, the $R\bar{3}m$-2 and $R\bar{3}m$-3 phases might also be produced in experiment, perhaps upon heating, which might overcome the big barriers between Si_3C and Si+C or Si+SiC.

The experimentally synthesized $Si_{0.75}C_{0.25}$ alloy with a diamond type structure at 1 atm is encouraging in this regard. As suggested by Qin et al.,[7] a transition metal might be used as a catalyst. Molybdenum would be worth trying, as it plays a crucial role in the growth process of the $Si_{1-x}C_x$ alloy. We note also that $Si_{80}C_{20}$ has been synthesized by using as a carbon source tetrasilylmethane, $C(SiH_3)_4$.[8] And it was proposed that Si_3C might also be synthesized from an analogous molecular precursor, $C_2(SiH_3)_6$.[38] The suggested crystal structures for Si_4C and Si_3C are both diamond-like (see Figure S6 in the SI), although there is C−C bond in the proposed structure for Si_3C.[38]

Our calculations show that the suggested structure for Si_3C with a C−C bond is about 0.5 eV/Si_3C higher than our predicted $I\bar{4}2d$ structure (see Figure S7 in the SI). For Si_4C, our calculated enthalpy shows that it is stable relative to Si+C between 8 and 10.5 GPa, while it is still unstable with respect to SiC+Si within the whole pressure range studied (see Figure S8 in the SI).

The mechanical stability of $I\bar{4}2d$ was also checked by calculating the independent elastic constants C_{ij} (see Table S1 in the SI), which all satisfy the mechanical stability criteria for the tetragonal structure.[39] It is well-known that SiC[6,40] is extremely hard; this leads to its commercial use. The hardness of SiC compares with that of B_4C.[41−44] Our calculated Vickers hardness H_v[45−48] for $I\bar{4}2d$ Si_3C is 20 GPa, which suggests that it is a hard material but not that hard (as discussed in the SI, the Vickers hardness of SiC is substantially larger than that of Si_3C). The relative softness might be due to the elongated multicenter Si−Si bonds. However, $I\bar{4}2d$ Si_3C is computed to have a little better ductility, measured by B/G of 1.2, than that of 1.07 for β-SiC.

Interestingly, the diamond type structure for Si_3C is calculated to be a semiconductor with a direct band gap at Γ in the Brillouin zone (Figure 4a). The calculated band gap (computed

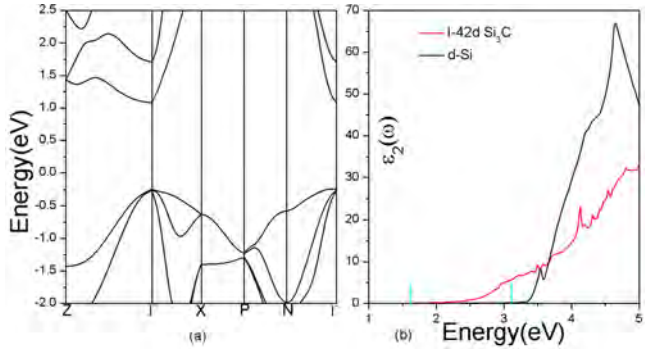

Figure 4. Electronic band structure and absorption spectra (imaginary part of dielectric function, ε_2) of Si_3C of $I\bar{4}2d$ Si_3C at 1 atm. The vertical light blue lines show the visible light range.

with a HSE hybrid functional[49,50] reasonably reliable for band gap estimates) is ∼1.3 eV. It is known that photovoltaic applications ideally require a direct band gap within 1.1−1.4 eV.[4,51] Our predicted diamond type structure, which is similar to the experimentally observed $Si_{0.75}C_{0.25}$ alloy, meets this requirement and might be a very good candidate for photovoltaic applications. To check for potential improvements in light absorption properties, we calculated absorption spectra (imaginary part of dielectric function, ε_2) of Si_3C at 1 atm, as shown in Figure 4b. The light absorption is significantly enhanced below 3.5 eV, compared with d-Si, particular in the visible light range.

The electronic band structure and density of states (DOS) of the $R\bar{3}m$-2 (Figure 5a,b) and $R\bar{3}m$-3 (Figure 5d,e) structures at 50 and 300 GPa indicate that they would be metallic. The square onset in the density of states in their lower energy range is consistent with their layered nature. From the projected DOS, we can see that the contribution from both 3p states of Si atoms and 2p states of C atoms are all big, and the contributions from 3s of Si atoms are also non-negligible. Around the Fermi level the states are derived mainly from 3s and 3p orbitals of Si atoms.

Further insight into the bonding may be obtained from calculating the −COHP (COHP = Crystal Orbital Hamilton Population; −COHP positive indicates bonding interactions) between various atom types (Figure 5c,f and Figure S4). This shows the clear and strong bonding between Si1,3-Si4 ($R\bar{3}m$-2), Si2,4-Si3 ($R\bar{3}m$-3), Si2,3-C ($R\bar{3}m$-2), and Si1,4-C ($R\bar{3}m$-3). Less obvious is the weak bonding between Si4−Si5 for $R\bar{3}m$-2 and $R\bar{3}m$-3.

The electronic DOS at the Fermi level in $R\bar{3}m$-1 (Figure S5), $R\bar{3}m$-2, and $R\bar{3}m$-3 (Figure 5) structures is quite high, compared to other materials we have studied. Encouragingly, well-known pure silicon will become superconducting under pressure.[52] These indications of potential superconductivity stimulated us

DOI: 10.1021/acs.chemmater.7b04243
Chem. Mater. 2018, 30, 421−427

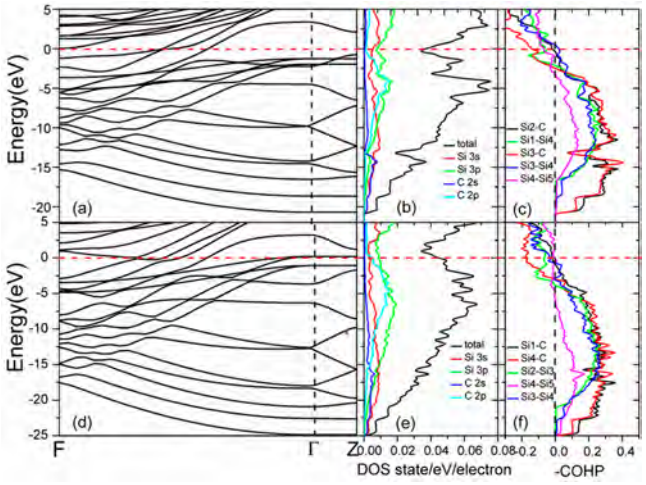

Figure 5. Electronic band structure (a, d), density of states (b, e), and COHP (c, f) between Si−Si and Si−C atoms of $R\bar{3}m$-2 and $R\bar{3}m$-3 Si_3C at 50 and 300 GPa, respectively. The horizontal dashed red line denotes the Fermi level. We plot the negative value of COHP to follow the convention of the chemical community.

to electron−phonon coupling (EPC) calculations for the $R\bar{3}m$-1 and $R\bar{3}m$-2 phases at 100 and 50 GPa, respectively. We did not calculate the EPC for the $R\bar{3}m$-3 structure, as its structure is very similar to the $R\bar{3}m$-2 phase.

As indicated earlier, the $R\bar{3}m$-1 and $R\bar{3}m$-2 phases are dynamically stable (Figure 6a,d) at 100 and 50 GPa, respectively. Note

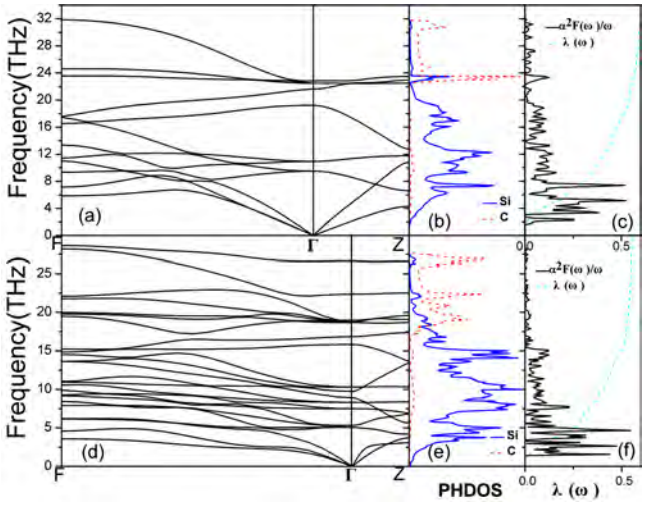

Figure 6. (a) and (d) Calculated phonon band structure for $R\bar{3}m$-1 and $R\bar{3}m$-2 Si_3C at 100 and 50 GPa, respectively. The Eliashberg phonon spectral function, $\alpha^2F(\omega)$, and the partial electron−phonon integral, $\lambda(\omega)$, in (C) and (f). (b) and (e) also show the Si and C contributions to the phonon DOS.

that the higher frequency motions are mostly of C atoms, while the lower frequency ones are of Si atoms. This is not surprising, as the silicons are heavier. The calculated EPC parameters (λ) are 0.6 and 0.5, and the logarithmic average phonon frequency (ω_{log}) is 414 and 298 K for $R\bar{3}m$-1 and $R\bar{3}m$-2, respectively. Using the Coulomb pseudopotential μ^* of 0.13,[53] the estimated T_c is 6.6 ($R\bar{3}m$-1) and 3.3 K ($R\bar{3}m$-2) based on the Allen-Dynes modified McMillan equation. T_c will change from 5 to 14 K and from 2.4 to 7.9K for $R\bar{3}m$-1, and $R\bar{3}m$-2, respectively, if μ^* were to be decreased from 0.15 to 0.06 (Figure 7). The calculated T_c

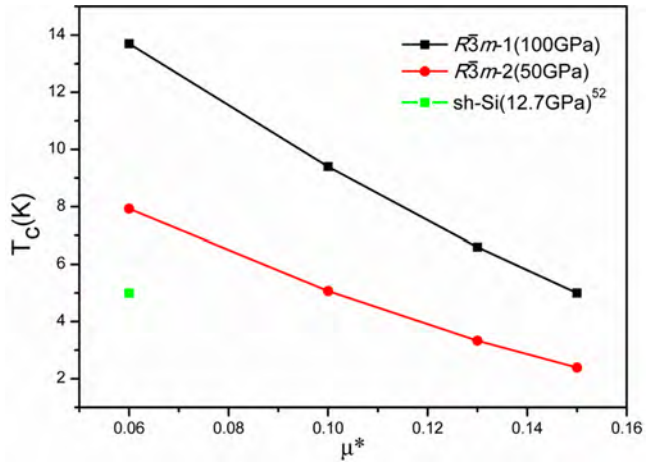

Figure 7. Calculated superconducting critical temperature T_c for $R\bar{3}m$-1, $R\bar{3}m$-2 and sh Si[52] at 100, 50, and 12.7 GPa, respectively, as a function of Coulomb pseudopotential parameter, μ^*.

for Si_3C under high pressure is higher than that of B-doped samples of 3C-SiC (1.4 K) and simple hexagonal (sh) silicon (5 K, calculated at 12.7 GPa by using μ^* of 0.06), respectively.[52,54−56]

CONCLUSION

We explored the crystal structures and properties of several new metastable Si_3C structures at 1 atm and under high pressure. At 1 atm, Si_3C adopts a diamond type structure, $I\bar{4}2d$. Under pressure, two $R\bar{3}m$-2 and $R\bar{3}m$-3 phases become stable; both phases are layered, with unusual octahedral 6-coordinate environments for C. $I\bar{4}2d$ Si_3C is calculated to be a very good semiconductor with a direct bandgap of 1.3 eV, with good optical properties. Under pressure, Si_3C transforms from a semiconductor to a metal. The higher pressure $R\bar{3}m$-1 and $R\bar{3}m$-2 Si_3C phases are calculated to be superconductors with T_c of a few Kelvins. This is the first time that one finds theoretically superconductivity in undoped silicon carbides.

ASSOCIATED CONTENT

Supporting Information

The Supporting Information is available free of charge on the ACS Publications website at DOI: 10.1021/acs.chemmater.7b04243.

Further details of computational methods, dynamical and electronic properties of Si_3C, Figures S1−S8, and Table S1 (PDF)

AUTHOR INFORMATION

Corresponding Authors

*(G.Y.G.) E-mail: gaoguoying@ysu.edu.cn.
*(R.H.) E-mail: rh34@cornell.edu.

ORCID

Guoying Gao: 0000-0003-3823-2942
Roald Hoffmann: 0000-0001-5369-6046

Notes

The authors declare no competing financial interest.

ACKNOWLEDGMENTS

We are grateful to the reviewers of this paper and V. Crespi, for their comments. The work at Yanshan University was supported by National Natural Science Foundation of China

DOI: 10.1021/acs.chemmater.7b04243
Chem. Mater. 2018, 30, 421−427

(Grant 11604290), the Science Foundation for the Youth Top-notch Talent from Universities of Hebei Province (Grant BJ2017023), Funding Program for Recruited Oversea Scholars of Hebei Province (CL201729), and PhD foundation by Yanshan University (Grant B970). The work at Cornell was supported by EFree (an Energy Frontier Research Center funded by the Department of Energy, Award Number DESC0001057 at Cornell). Computational resources provided by the XSEDE network (provided by the National Center for Supercomputer Applications through Grant TG-DMR060055N) and by Cornell's NanoScale Facility (supported by the National Science Foundation through Grant ECS-0335765) are gratefully acknowledged.

REFERENCES

(1) Hybertsen, M. S.; Louie, S. G. First-principles theory of quasiparticles: Calculation of band gaps in semiconductors and insulators. *Phys. Rev. Lett.* **1985**, *55* (13), 1418−1421.
(2) Wang, Q.; Xu, B.; Sun, J.; Liu, H.; Zhao, Z.; Yu, D.; Fan, C.; He, J. Direct band gap silicon allotropes. *J. Am. Chem. Soc.* **2014**, *136* (28), 9826.
(3) Xiang, H. J.; Huang, B.; Kan, E.; Wei, S. H.; Gong, X. G. Towards direct-gap silicon phases by the inverse band structure design approach. *Phys. Rev. Lett.* **2013**, *110* (11), 118702.
(4) Rühle, S. Tabulated values of the Shockley−Queisser limit for single junction solar cells. *Sol. Energy* **2016**, *130*, 139−147.
(5) Kim, D. Y.; Stefanoski, S.; Kurakevych, O. O.; Strobel, T. A. Synthesis of an open-framework allotrope of silicon. *Nat. Mater.* **2015**, *14* (2), 169−73.
(6) Willardson, R. K.; Weber, E. R.; Park, Y. S. *SiC materials and devices*; Academic Press: New York, 1998.
(7) Qin, W.; Wu, C.; Qin, G.; Zhang, J.; Zhao, D. Highly Concentrated Alloy with an Ordered Superstructure. *Phys. Rev. Lett.* **2003**, *90* (24), 245503.
(8) Kouvetakis, J.; Chandrasekhar, D.; Smith, D. J. Growth and characterization of thin $Si_{80}C_{20}$ films based upon Si_4C building blocks. *Appl. Phys. Lett.* **1998**, *72* (8), 930−932.
(9) Kouvetakis, J.; Nesting, D.; Smith, D. J. Synthesis and Atomic and Electronic Structure of New Si−Ge−C Alloys and Compounds. *Chem. Mater.* **1998**, *10* (10), 2935−2949.
(10) Khaenko, B.; Prilutskii, E.; Mikhailik, A.; Karpets, M. Formation of a new phase upon heating of the products of interaction of SiC with SiO_2. *Powder Metall. Met. Ceram.* **1996**, *34* (9), 513−514.
(11) Guo, L.; Wang, Y.; Song, F.; He, F.; Huang, Y.; Yan, L.; Wan, Y. Formation and characterization of Si_5C_3 type silicon carbide by carbon ion implantation with a MEVVA ion source. *Mater. Lett.* **2007**, *61* (19), 4083−4085.
(12) Dube, C. L.; Kashyap, S. C.; Dube, D. C.; Agarwal, D. K. Growth of $Si_{0.75}Ge_{0.25}$ alloy nanowires in a separated H-field by microwave processing. *Appl. Phys. Lett.* **2009**, *94* (21), 213107.
(13) Rahman, M. M.; Zhang, S.; Tambo, T.; Tatsuyama, C. Structural Characterization of $Si_{0.75}Ge_{0.25}$ Alloy Layers with Sb/Ge-Mediated Low Temperature-grown Si Buffers. *Jpn. J. Appl. Phys.* **2005**, *44* (5A), 2967−2970.
(14) Basu, R.; Bhattacharya, S.; Bhatt, R.; Roy, M.; Ahmad, S.; Singh, A.; Navaneethan, M.; Hayakawa, Y.; Aswal, D. K.; Gupta, S. K. Improved thermoelectric performance of hot pressed nanostructured n-type SiGe bulk alloys. *J. Mater. Chem. A* **2014**, *2* (19), 6922−6930.
(15) Bathula, S.; Jayasimhadri, M.; Dhar, A. Mechanical properties and microstructure of spark plasma sintered nanostructured p-type SiGe thermoelectric alloys. *Mater. Des.* **2015**, *87*, 414−420.
(16) Kinoshita, K.; Arai, Y.; Inatomi, Y.; Miyata, H.; Tanaka, R.; Sone, T.; Yoshikawa, J.; Kihara, T.; Shibayama, H.; Kubota, Y.; et al. Homogeneous SiGe crystal growth in microgravity by the travelling liquidus-zone method. *J. Phys.Conf. Ser.* **2011**, *327*, 012017.
(17) Gao, G.; Ashcroft, N. W.; Hoffmann, R. The unusual and the expected in the Si/C phase diagram. *J. Am. Chem. Soc.* **2013**, *135* (31), 11651.
(18) Wang, Y.; Lv, J.; Zhu, L.; Ma, Y. Crystal structure prediction via particle-swarm optimization. *Phys. Rev. B: Condens. Matter Mater. Phys.* **2010**, *82* (9), 094116.
(19) Wang, Y.; Lv, J.; Zhu, L.; Ma, Y. CALYPSO: A method for crystal structure prediction. *Comput. Phys. Commun.* **2012**, *183* (10), 2063−2070.
(20) Li, Y.; Hao, J.; Liu, H.; Li, Y.; Ma, Y. The metallization and superconductivity of dense hydrogen sulfide. *J. Chem. Phys.* **2014**, *140* (17), 174712.
(21) Lv, J.; Wang, Y.; Zhu, L.; Ma, Y. Predicted novel high-pressure phases of lithium. *Phys. Rev. Lett.* **2011**, *106* (1), 015503.
(22) Zhu, L.; Liu, H.; Pickard, C. J.; Zou, G.; Ma, Y. Reactions of xenon with iron and nickel are predicted in the Earth's inner core. *Nat. Chem.* **2014**, *6* (7), 644.
(23) Kresse, G.; Furthmüller, J. Efficient iterative schemes for ab initio total-energy calculations using a plane-wave basis set. *Phys. Rev. B: Condens. Matter Mater. Phys.* **1996**, *54* (16), 11169−11186.
(24) Perdew, J. P.; Chevary, J. A.; Vosko, S. H.; Jackson, K. A.; Pederson, M. R.; Singh, D. J.; Fiolhais, C. Atoms, molecules, solids, and surfaces: Applications of the generalized gradient approximation for exchange and correlation. *Phys. Rev. B: Condens. Matter Mater. Phys.* **1992**, *46* (11), 6671−6687.
(25) Dronskowski, R.; Bloechl, P. E. Crystal orbital Hamilton populations (COHP): energy-resolved visualization of chemical bonding in solids based on density-functional calculations. *J. Phys. Chem.* **1993**, *97* (33), 8617−8624.
(26) Deringer, V. L.; Tchougreeff, A. L.; Dronskowski, R. Crystal orbital Hamilton population (COHP) analysis as projected from plane-wave basis sets. *J. Phys. Chem. A* **2011**, *115* (21), 5461.
(27) Maintz, S.; Deringer, V. L.; Tchougreeff, A. L.; Dronskowski, R. LOBSTER: A tool to extract chemical bonding from plane-wave based DFT. *J. Comput. Chem.* **2016**, *37* (11), 1030.
(28) Parlinski, K.; Li, Z. Q.; Kawazoe, Y. First-Principles Determination of the Soft Mode in Cubic ZrO_2. *Phys. Rev. Lett.* **1997**, *78* (21), 4063−4066.
(29) Togo, A.; Oba, F.; Tanaka, I. First-principles calculations of the ferroelastic transition between rutile-type and $CaCl_2$-type SiO_2 at high pressures. *Phys. Rev. B: Condens. Matter Mater. Phys.* **2008**, *78* (13), 134106.
(30) Giannozzi, P.; Baroni, S.; Bonini, N.; Calandra, M.; Car, R.; Cavazzoni, C.; Ceresoli, D.; Chiarotti, G. L.; Cococcioni, M.; Dabo, I.; et al. QUANTUM ESPRESSO: a modular and open-source software project for quantum simulations of materials. *J. Phys.: Condens. Matter* **2009**, *21* (39), 395502.
(31) Fahy, S.; Louie, S. G. High-pressure structural and electronic properties of carbon. *Phys. Rev. B: Condens. Matter Mater. Phys.* **1987**, *36* (6), 3373−3385.
(32) Scandolo, S.; Chiarotti, G. L.; Tosatti, E. SC4: A metallic phase of carbon at terapascal pressures. *Phys. Rev. B: Condens. Matter Mater. Phys.* **1996**, *53* (9), 5051−5054.
(33) Lee, M. S.; Montoya, J. A.; Scandolo, S. Thermodynamic stability of layered structures in compressed CO_2. *Phys. Rev. B: Condens. Matter Mater. Phys.* **2009**, *79* (14), 144102.
(34) Yoshida, M.; Onodera, A.; Ueno, M.; Takemura, K.; Shimomura, O. Pressure-induced phase transition in SiC. *Phys. Rev. B: Condens. Matter Mater. Phys.* **1993**, *48* (14), 10587.
(35) Hatch, D. M.; Stokes, H. T.; Dong, J.; Gunter, J.; Wang, H.; Lewis, J. P. Bilayer sliding mechanism for the zinc-blende to rocksalt transition in SiC. *Phys. Rev. B: Condens. Matter Mater. Phys.* **2005**, *71* (18), 184109.
(36) Daviau, K.; Lee, K. K. M. Zinc-blende to rocksalt transition in SiC in a laser-heated diamond-anvil cell. *Phys. Rev. B: Condens. Matter Mater. Phys.* **2017**, *95* (13), 134108.
(37) Muetterties, E. L. *The chemistry of boron and its compounds*; Wiley: New York, 1967.
(38) Zhang, P.; Crespi, V. H.; Chang, E.; Louie, S. G.; Cohen, M. L. Theory of metastable Group-IV alloys formed from CVD precursors. *Phys. Rev. B: Condens. Matter Mater. Phys.* **2001**, *64* (23), 235201.

DOI: 10.1021/acs.chemmater.7b04243
Chem. Mater. 2018, 30, 421−427

(39) Watt, J. P.; Peselnick, L. Clarification of the Hashin-Shtrikman bounds on the effective elastic moduli of polycrystals with hexagonal, trigonal, and tetragonal symmetries. *J. Appl. Phys.* **1980**, *51* (3), 1525−1531.
(40) Brazhkin, V. V.; Lyapin, A. G.; Hemley, R. J. Harder than diamond: Dreams and reality. *Philos. Mag. A* **2002**, *82* (2), 231−253.
(41) An, Q.; Goddard, W. A., III Microalloying Boron Carbide with Silicon to Achieve Dramatically Improved Ductility. *J. Phys. Chem. Lett.* **2014**, *5* (23), 4169.
(42) An, Q.; Goddard, W. A., III; Cheng, T. Atomistic explanation of shear-induced amorphous band formation in boron carbide. *Phys. Rev. Lett.* **2014**, *113* (9), 095501.
(43) Thévenot, F. Boron carbide—A comprehensive review. *J. Eur. Ceram. Soc.* **1990**, *6* (4), 205−225.
(44) Moshtaghioun, B. M.; Gomez-Garcia, D.; Dominguez-Rodriguez, A.; Todd, R. I. Grain size dependence of hardness and fracture toughness in pure near fully-dense boron carbide ceramics. *J. Eur. Ceram. Soc.* **2016**, *36* (7), 1829−1834.
(45) Tian, Y.; Xu, B.; Zhao, Z. Microscopic theory of hardness and design of novel superhard crystals. *Int. J. Refract. Hard Met.* **2012**, *33* (33), 93−106.
(46) Zhao, Z.; Xu, B.; Tian, Y. Recent Advances in Superhard Materials. *Annu. Rev. Mater. Res.* **2016**, *46* (1), 383.
(47) Gao, F.; He, J.; Wu, E.; Liu, S.; Yu, D.; Li, D.; Zhang, S.; Tian, Y. Hardness of covalent crystals. *Phys. Rev. Lett.* **2003**, *91* (1), 015502.
(48) He, J.; Wu, E.; Wang, H.; Liu, R.; Tian, Y. Ionicities of Boron-Boron Bonds in B_{12} Icosahedra. *Phys. Rev. Lett.* **2005**, *94* (1), 015504.
(49) Heyd, J.; Scuseria, G. E. Efficient hybrid density functional calculations in solids: assessment of the Heyd-Scuseria-Ernzerhof screened Coulomb hybrid functional. *J. Chem. Phys.* **2004**, *121* (3), 1187.
(50) Heyd, J.; Scuseria, G. E.; Ernzerhof, M. Hybrid functionals based on a screened Coulomb potential. *J. Chem. Phys.* **2003**, *118* (18), 8207−8215.
(51) Shockley, W.; Queisser, H. J. Detailed Balance Limit of Efficiency of p-n Junction Solar Cells. *J. Appl. Phys.* **1961**, *32* (3), 510−519.
(52) Chang, K. J.; Dacorogna, M. M.; Cohen, M. L.; Mignot, J. M.; Chouteau, G.; Martinez, G. Superconductivity in High-Pressure Metallic Phases of Si. *Phys. Rev. Lett.* **1985**, *54* (21), 2375−2378.
(53) Ashcroft, N. W. Metallic Hydrogen: A High-Temperature Superconductor? *Phys. Rev. Lett.* **1968**, *21* (26), 1748−1749.
(54) Ren, Z.-A.; Kato, J.; Muranaka, T.; Akimitsu, J.; Kriener, M.; Maeno, Y. Superconductivity in Boron-doped SiC. *J. Phys. Soc. Jpn.* **2007**, *76* (10), 103710.
(55) Muranaka, T.; Kikuchi, Y.; Yoshizawa, T.; Shirakawa, N.; Akimitsu, J. Superconductivity in carrier-doped silicon carbide. *Sci. Technol. Adv. Mater.* **2008**, *9* (4), 044204.
(56) Kriener, M.; Muranaka, T.; Kato, J.; Ren, Z. A.; Akimitsu, J.; Maeno, Y. Superconductivity in heavily boron-doped silicon carbide. *Sci. Technol. Adv. Mater.* **2008**, *9* (4), 044205.

DOI: 10.1021/acs.chemmater.7b04243
Chem. Mater. 2018, 30, 421−427